

RESEARCH ARTICLE

10.1002/2013WR014593

Special Section:

Patterns in Soil-Vegetation-
Atmosphere Systems:
Monitoring, Modelling and
Data Assimilation

Key Points:

- The relation between resistivity data and geological units is largely uncertain
- AEM data show advantage for transition probability in the horizontal direction
- The selection of conditioning method is critical for geostatistical simulations

Correspondence to:

X. He,
xhe@geus.dk

Citation:

He, X., J. Koch, T. O. Sonnenborg, F. Jørgensen, C. Schamper, and J. Christian Refsgaard (2014), Transition probability-based stochastic geological modeling using airborne geophysical data and borehole data, *Water Resour. Res.*, *50*, 3147–3169, doi:10.1002/2013WR014593.

Received 16 AUG 2013

Accepted 19 MAR 2014

Accepted article online 25 MAR 2014

Published online 10 APR 2014

Transition probability-based stochastic geological modeling using airborne geophysical data and borehole data

Xin He¹, Julian Koch¹, Torben O. Sonnenborg¹, Flemming Jørgensen², Cyril Schamper³, and Jens Christian Refsgaard¹

¹Department of Hydrology, Geological Survey of Denmark and Greenland, Copenhagen, Denmark, ²Department of Groundwater and Quaternary Geological Mapping, Geological Survey of Denmark and Greenland, Aarhus, Denmark, ³Department of Geoscience, University of Aarhus, Aarhus, Denmark

Abstract Geological heterogeneity is a very important factor to consider when developing geological models for hydrological purposes. Using statistically based stochastic geological simulations, the spatial heterogeneity in such models can be accounted for. However, various types of uncertainties are associated with both the geostatistical method and the observation data. In the present study, TProGS is used as the geostatistical modeling tool to simulate structural heterogeneity for glacial deposits in a head water catchment in Denmark. The focus is on how the observation data uncertainty can be incorporated in the stochastic simulation process. The study uses two types of observation data: borehole data and airborne geophysical data. It is commonly acknowledged that the density of the borehole data is usually too sparse to characterize the horizontal heterogeneity. The use of geophysical data gives an unprecedented opportunity to obtain high-resolution information and thus to identify geostatistical properties more accurately especially in the horizontal direction. However, since such data are not a direct measurement of the lithology, larger uncertainty of point estimates can be expected as compared to the use of borehole data. We have proposed a histogram probability matching method in order to link the information on resistivity to hydrofacies, while considering the data uncertainty at the same time. Transition probabilities and Markov Chain models are established using the transformed geophysical data. It is shown that such transformation is in fact practical; however, the cutoff value for dividing the resistivity data into facies is difficult to determine. The simulated geological realizations indicate significant differences of spatial structure depending on the type of conditioning data selected. It is to our knowledge the first time that grid-to-grid airborne geophysical data including the data uncertainty are used in conditional geostatistical simulations in TProGS. Therefore, it provides valuable insights regarding the advantages and challenges of using such comprehensive data.

1. Introduction

The success of groundwater flow simulation is largely determined by the conceptualization of the geology. Geological models developed for hydrological purposes are traditionally derived from stratigraphical interpretations of direct and/or indirect observations, each associated with various resolution, and types and magnitudes of uncertainties [James and Freeze, 1993; Mclaughlin et al., 1993; Berkowitz, 2002; Feyen and Caers, 2006; Refsgaard et al., 2012]. It is suggested by several studies that the resulting geological structural uncertainty plays an important role, especially in simulations beyond fluid flow, for instance, the simulation of contaminant transport. It is crucial that realistic geological structures are used in such cases since the flow paths may be mistaken even though the water budget is simulated correctly [Selroos et al., 2002; Højberg and Refsgaard, 2005; Poeter and Anderson, 2005; Trolldborg et al., 2007; Rojas et al., 2008; Seifert et al., 2008].

The geological model used in groundwater simulations, including layers, units, etc., is traditionally constructed using a deterministic geological interpretation, which assembles the most comprehensive knowledge available for the site being investigated [Sophocleous et al., 1999; Henriksen et al., 2003; Kollet and Maxwell, 2006; Lemieux et al., 2008]. Using this approach, the hydrological predictive uncertainty originating from the geological structural uncertainty is typically unaccounted for. It is possible to replace the geological structural uncertainty by effective parameter uncertainty through inverse calibration of hydrological model parameters [Hill and Tiedeman, 2007]. However, the parameter values obtained through calibration with a biased geological model are also biased. Therefore, deterministic models with biased parameter values are unable to make accurate predictions for conditions outside the calibration base.

It is commonly acknowledged that the geological structural uncertainty can be evaluated by using several equally plausible models, and such geological models can be constructed manually and/or stochastically [Franssen and Gomez-Hernandez, 2002; Højberg and Refsgaard, 2005; Trolborg et al., 2010; Seifert et al., 2012]. Generating multiple geological models using the stochastic approach requires the use of geostatistical modeling tools.

Geostatistical techniques for generating multiple geological realizations have become increasingly accessible in recent years [Deutsch and Cockerham, 1994; Carle and Fogg, 1996; Goovaerts, 2001; Strebelle, 2002; Poeter and Anderson, 2005; Refsgaard et al., 2006]. Among these techniques, Transition Probability Geostatistical Software (TProGS) is a two-point geostatistical method that is able to reproduce critical hydrogeological features, such as the volumetric proportions, the mean lengths, and the juxtapositional tendencies of the facies [Carle and Fogg, 1996; Carle, 1997; Weissmann and Fogg, 1999; Ritzi, 2000; Engdahl et al., 2010a; dell'Arciprete et al., 2012]. TProGS also provides an extension to the traditional variogram analysis, especially for asymmetrical structures where the geological characteristics may not be captured by simply using a variogram model [Lee et al., 2007]. The multipoint geostatistics have shown promising improvement compared to the traditional two-point geostatistics. However, it requires that a 3-D training image exists which adequately represents the geological heterogeneity of the entire model domain [Hu and Chuginova, 2008].

The TProGS package produces stochastic geological realizations through Sequential Indicator Simulation (SIS) and Quenching. SIS is widely used in soil surveys, reservoir modeling, and hydrogeological investigations where the nature of the data is primarily categorical [Sminchak et al., 1996; Juang et al., 2004; Elfeki and Dekking, 2007; de Almeida, 2010; Quental et al., 2012]. Recent studies have demonstrated the possibility of incorporating conditional data in SIS, such that the random process also honors reference data at specific locations [McKenna and Poeter, 1995; Lee et al., 2007; Engdahl et al., 2010b; dell'Arciprete et al., 2012]. In conditional stochastic simulations, one can either force the realizations to honor the data completely, "hard conditioning," or to honor the data partly with consideration of the uncertainty of the data, "soft conditioning" [Carle et al., 2006; Falivene et al., 2007]. However, it is not resolved how subjective information can be used properly in geostatistical simulation.

Typically, the geostatistical characteristics in TProGS are established using borehole data. Borehole data provide adequate information on the distribution and variability of the deposits in the vertical direction, but provide relatively weak information in the horizontal direction, since the horizontal length scale of lithological units is usually smaller than the spacing between the wells in heterogeneous media. To overcome this problem, studies have attempted to include spatially distributed but indirect information on geology for solving data scarcity issues in the horizontal direction [Weissmann and Fogg, 1999; Elfeki, 2006; Harp et al., 2008; Ye and Khaleel, 2008].

Previously, spatial geophysical data such as Ground Penetrating Radar (GPR) or seismic data have been employed in geological simulations using various types of geostatistical techniques [Parra et al., 2006; Engdahl et al., 2010b; De Benedetto et al., 2012]. In the present study, data obtained from an Airborne transient ElectroMagnetic (AEM) survey are used to assist stochastic geological simulation using TProGS in a headwater catchment in western Denmark. The transient EM method uses the inductive response of the ground that is generated after the abrupt turn off of the electric current in a transmitter wired loop to relate the decay of the magnetic field to the resistivity distribution of the ground. The conductive layers such as clays provide the strongest responses, and the observation of the decay from the early times (i.e., right after the turn off of the current) to the late times gives information from the near surface to the deeper formations [Ward and Hohmann, 1988; Christiansen et al., 2006]. The transient AEM system used in the present study, SkyTEM, was initially designed for groundwater investigations and has been improved successively, leading to different versions of the system with different size and power [Christiansen and Christensen, 2003; Sørensen and Auken, 2004; Auken et al., 2009; Kirkegaard et al., 2011]. Each version is adapted to the target's depth, the most powerful version allowing prospection down to several hundred meters (larger electrical resistivities in the top favoring deeper penetration of the EM field), and the smallest and less powerful system providing a better resolution of the near surface.

The specific SkyTEM version used in the present study is called SkyTEM101. It has been developed to deliver very high resolution in the near surface (top 20 m; C. Schamper et al., Assessment of near-surface mapping capabilities by airborne transient electromagnetic data—An extensive comparison to conventional borehole

data, submitted to *Geophysics*, 2013). The new processing methodology applied to this system for improving near-surface resolution is detailed in *Schamper et al.* [2014]. Despite its near-surface oriented design, the SkyTEM101 system still has a depth of investigation of 100 m for a medium resistivity of 50 Ω m. SkyTEM data have the potential to become an important source of information in the construction of 3-D transition probability/Markov Chain models. Additionally, the density of SkyTEM data provides a unique opportunity for conditional geostatistical simulations. However, the added value of the extra conditional data on the geological simulations still needs to be analyzed.

There are a number of known limitations and uncertainties associated with the use of transient AEM data as a proxy of the geology, e.g., vertical and horizontal resolution capability, variations in ion content of pore water and coupled and noise-infected data [*Jørgensen et al.*, 2012, 2013; *Viezzoli et al.*, 2013]. As a result, when geostatistical simulations are carried out with the purpose to generate hydrogeological models, AEM data may be best used indirectly as soft data. Borehole data, on the other hand, are in situ and generally convenient to use. However, the borehole data may also be associated with various types of uncertainties. Therefore, how to incorporate the uncertainties from the observation data, including both the geological and geophysical data, remains an important challenge.

The objectives of the present study are: (1) to develop a method that transforms AEM data so that they can be used in stochastic geological simulations by establishing a relationship between the facies data based on borehole logs and the resistivity data based on the AEM survey; (2) to simulate equally likely geological realizations using the transition probability-based indicator geostatistics with both borehole and AEM data as soft conditioning; and (3) to analyze the uncertainties in the stochastic simulations with regard to data types and different conditioning approaches. The result of the study gives information about the strengths and weaknesses of the geostatistical software used, and it also underlines the importance of conditioning data in such geological simulations.

2. Materials and Methods

The Norsminde Fjord catchment is selected as the study area. Two types of field data, namely borehole data and AEM data, are extracted from the national geological database and collected from a field campaign, respectively. A method is developed in order to link these two types of data, so the remotely sensed geophysical data can also be used in simulations of geological facies. The stochastic geological modeling tool used is TProGS [*Carle*, 1996].

2.1. Study Area and Geology

The Norsminde Fjord catchment located on the east coast of Jutland peninsula in Denmark (Figure 1) is selected as the study site. The headwater catchment drains to Aarhus Bay through Raevs River and numerous small tributaries. Over 70% of the drainage area is intensively farmed agricultural land. The catchment slopes from west to east with about 90 m difference in surface elevation.

Knowledge of the geological and hydrogeological setting is mainly derived from groundwater abstraction wells. In general, the setting encompasses Paleogene and Neogene marine sediments covered by heterogeneous sequences of Pleistocene glacial deposits. The Paleogene layers are mainly of hemiplegic origin and composed of very fine-grained impermeable marl and clay. The Neogene layers above comprise a clay-dominated, Miocene marine formation interbedded by sandy deltaic units. These sand units can reach thicknesses of more than 10 m, and the entire Miocene sequence is typically up to 40 m thick [*Rasmussen et al.*, 2010]. The Miocene is only present in the western part of the area, and the Paleogene clay is therefore directly covered by the glacial deposits in the eastern part. The Paleogene and Miocene deposits are in places incised by deep buried tunnel valleys, in particular, in the southern part where the Boulstrup valley crosses the model area [*Jørgensen and Sandersen*, 2006].

The glacial deposits are composed of both sandy and clayey sediments. According to the boreholes, the clay layers include a variety of lithologies from glaciolacustrine clay to clay till. The sandy glacial deposits are generally of glaciofluvial origin and seem to occur as distributed and relatively small units within the clay-dominated environment. The sequence is occasionally heavily deformed with occurrences of rafts of Paleogene clay. The western part of the glacial sequence is subjected to stochastic geological modeling, as shown in Figure 1. This area is delineated from the remaining area on the basis of surface morphology in which a heavily deformed area occurs toward the northwest. Toward the east the glacial sequence

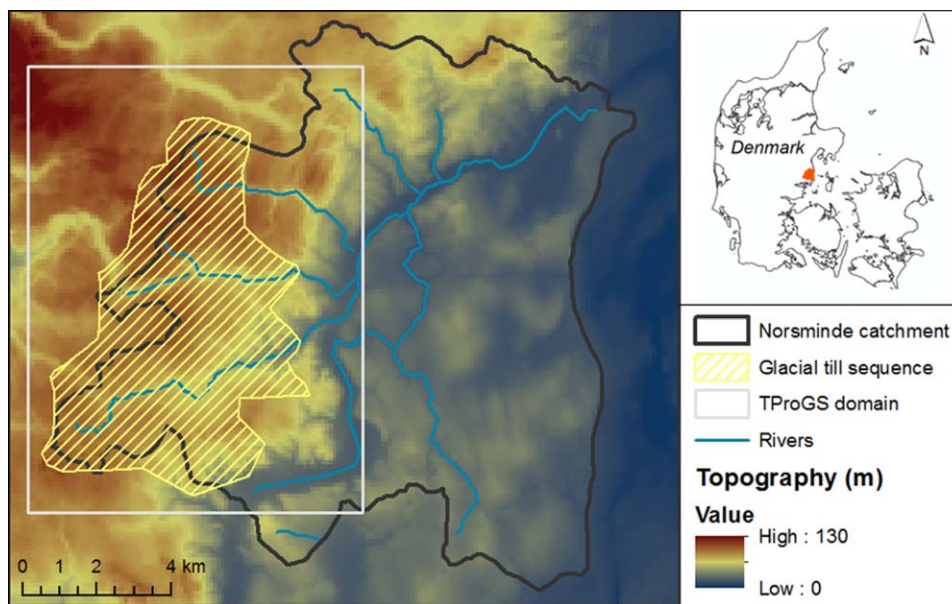


Figure 1. Location of the study area and the subarea with the glacial till deposit (shaded area) that is considered in the geostatistical simulations. The domain used in TProGS is denoted by the white rectangle.

pinches out due to surface erosion and to the south and west it is bounded by the limit of the survey area. The lower boundary is delineated on the basis of borehole information. The contact between Miocene deposits and glacial deposits has been identified in each borehole and these positions have subsequently been interpolated into a grid to represent the spatial structure of the boundary. The glacial till sequence is singled out to ensure that all geological processes comply with a weak stationarity assumption in this sub volume, and therefore does not impose any significant trend in space. The area of the modeling domain is 108 km².

2.2. Borehole Data and Quality Rating

Borehole information is obtained from the Danish National Geological Database—Jupiter, which contains information on the 177 boreholes in the modeling area (Figure 2). All the boreholes have been automatically assigned to quality groups by running a set of dedicated database queries. Each borehole is classified into quality group 1 through 5, where group 1 refers to the highest quality and group 5 refers to very low quality or no data. Boreholes from group 5 are discarded from the subsequent calculations.

The basic principle in the borehole rating is to separate the boreholes that are able to provide accurate and useful information on lithology from the boreholes that provide very little information or even misleading information. The rating is focused on the boreholes’ ability to distinguish between sand and clay, and the ability to identify the exact locations of layer boundaries between sand and clay units. It is preferable if procedures to assess quantitative rating scores are established such that borehole ratings can be compared to other areas and the results can be used directly for model constraining.

Six main criteria that directly or indirectly influence the quality of lithological borehole data are taken into consideration, including:

1. Accuracy of the geographical position, i.e., boreholes with coordinates determined by GPS, are rated higher than other boreholes.
2. Drilling method and purpose, i.e., auger drillings are rated higher than mud circulation drillings, and boreholes drilled for drinking water purposes are rated higher than boreholes drilled for seismic data collection.
3. Credibility of the contractors, i.e., boreholes drilled by drillers with a good reputation is rated higher than boreholes drilled by drillers with a bad reputation.
4. Abundance of registered samples, i.e., boreholes with many samples per drilled depth distance is rated higher than boreholes with few samples.

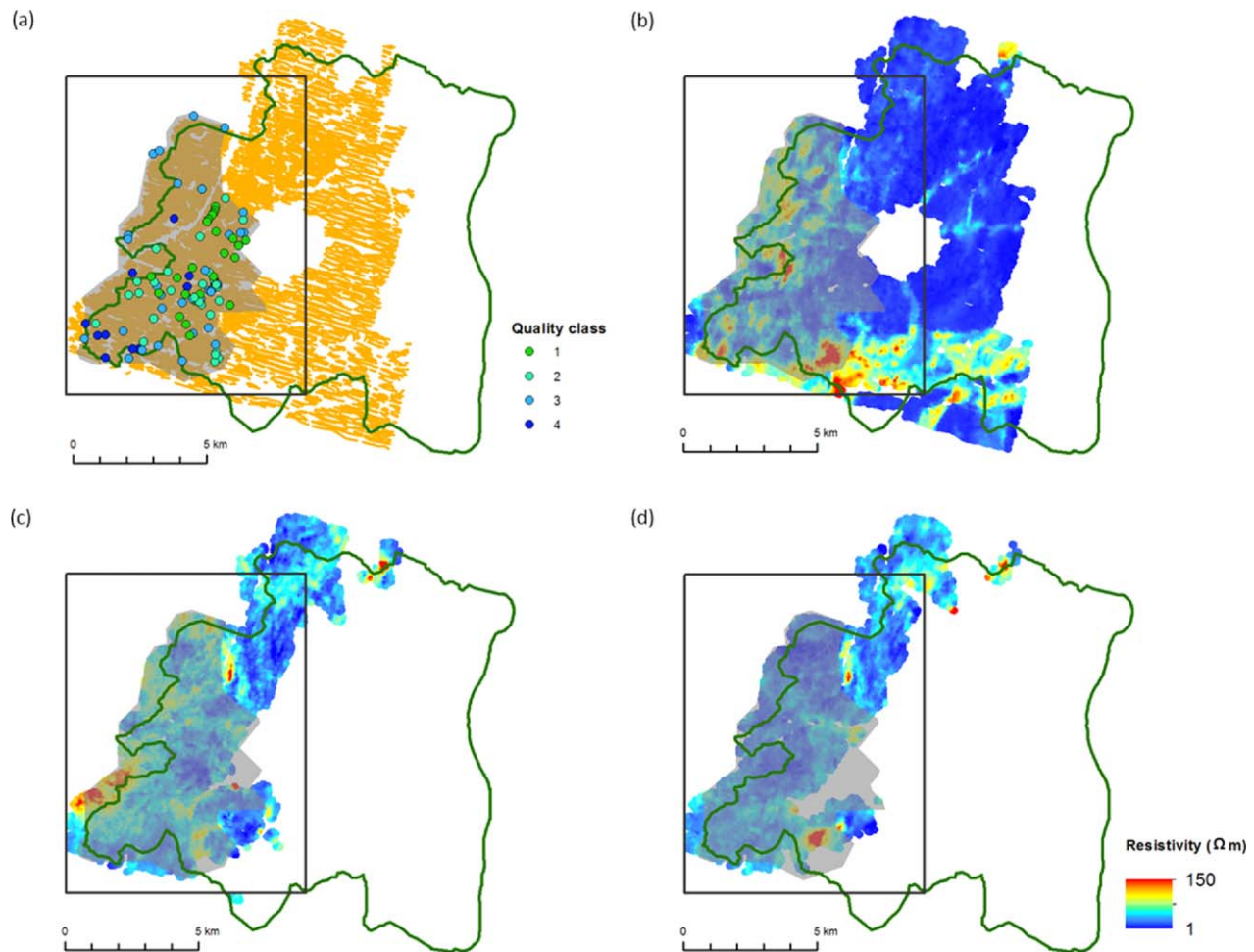


Figure 2. Observation data used in TProGS simulations. (a) Location of the boreholes as well as their affiliated quality groups, see Table 3. The SkyTEM flight lines after processing with different flight densities are also shown; and (b–d) illustration of interpolated SkyTEM data onto $20\text{ m} \times 20\text{ m} \times 2\text{ m}$ grid using point sounding data at 0, 49, and 59 m. The TProGS model domain as well as the glacial till sequence is the same as indicated in Figure 1. Note that the glacial till sequence is located above elevations of 0 m.

5. Age of the borehole, i.e., young boreholes are rated higher than old boreholes.

6. Occurrence of major errors, i.e., boreholes with a high discrepancy between registered elevation and the elevation of the ground surface at the registered drilling site are rated low.

The influence of each factor is counted and individual scores are assigned. The evaluation is concluded with an overall rating that sums up the individual scores from all the contributing factors.

Although lithological units can be read directly from the borehole log data, the number of lithological units is usually too great to be used directly in categorical geostatistical modeling. Thus, borehole lithological data are converted into a textual facies system, which usually consists of fewer categories such as sand and clay. In this context, facies is defined as a group of soil that shares similar hydraulic properties. In the present study, we consider two facies, namely sand and clay.

2.3. The SkyTEM Survey

Airborne geophysical data were collected in the Norsminde catchment in June 2011 during a week-long field campaign. After processing the voltage data from the SkyTEM helicopter campaign, which in principle consists of the culling of the sounding perturbed by coupling due to the presence of man-made installations (e.g., power lines, buried pipes), the AEM data are processed using a spatially constrained inversion algorithm [Viezzoli *et al.*, 2009]. The results provide a quasi-3-D distribution of both the near-surface (top 20 m) and the deep (down to 100 m) resistivity. The sounding points are distributed along the flight lines and over 29 fixed

depths relative to the ground surface. Altogether there are nearly 2000 km of flight lines and over 100,000 sounding positions in the Norsminde catchment. The spacing between the flight lines is maximum 100 m, and on the west side of the catchment denser flight lines with a spacing of approximately 50 m have been used, as shown in Figure 2. The target area is located at the place where the flight lines are most dense.

Point sounding data represent the measurement over a certain volume (e.g., upper layer footprint can be 25–75 m); therefore in order to compare resistivity data directly with local lithological data, interpolated sounding data are used instead. Consequently, gridded resistivity data with dimensions of 20 m × 20 m horizontally and 2 m vertically are generated as successive horizontal slices after 2-D interpolation of point sounding data using kriging.

2.4. Linking Facies Probabilities to Resistivity

In order to use the AEM data in stochastic geological indicator simulations, the inverted resistivity data need to be expressed as facies types [Gunnink and Siemon, 2009; Gunnink et al., 2012]. A procedure is developed for connecting airborne TEM data to the information on facies obtained from borehole well logs; this procedure uses a histogram probability matching method (HPMM):

$$P(I|R[r_1, r_2]) = \int_{r_1}^{r_2} f(R) \cdot dR \tag{1}$$

$$\sum_0^I P(I) = 1$$

where I is a certain facies category, and R is the resistivity measured by the AEM system, r_1 and r_2 are the starting and finishing point of each resistivity interval, and $f(R)$ is the function that transforms a resistivity value to a sand probability. Equation (1) assumes that the probability of getting facies I is positively correlated to the occurrence of resistivity over a certain range. To implement this idea and also to simplify the problem, resistivity data, which is in reality a continuous variable, are divided into discrete intervals. A fixed vertical discretization is defined based on the scale of the presumed thinnest unit in the study area. The categorical data from the boreholes are paired with the interpolated sounding data at the same coordinates. Next, a bin width is chosen to group the resistivity data. The bin width has to be large enough to ensure that a sufficient number of pairs of data types are available in each bin, and small enough to ensure a minimum resolution of the histogram. The percentage of a facies is then calculated for each bin. Lastly, a curve fitting is performed to characterize the shape of the histogram. The probability of the facies is an indication of data hardness with any given resistivity value. In the HPMM approach, a transition zone is usually defined in order to represent the transition from one pure facies to another pure facies. However, in case the histogram is very flat indicating that the link between the facies data and the resistivity data is very uncertain, the transition zone can also be subjectively defined as the high uncertainty zone which corresponds to a range of probability, e.g., 30%–70% of sand.

If the AEM data are used in a deterministic way, i.e., a fixed number of categories are provided without considering their uncertainty, cutoff values are needed. In such cases, the histogram gives a good opportunity to estimate where the cutoff values are likely to be located. In this study, only two categories are considered, and the cutoff value should be at the resistivity level that corresponds to 50% probability for the facies unit being studied. However, a precise cutoff value cannot always be determined in the HPMM approach since the cutoff value is usually located somewhere in the transition zone, and therefore subject to high uncertainty. An empirical way to overcome this problem is to implement a cost function:

$$f_c(\theta) = abs |p_m(I|\theta) - p_n(I)|$$

$$\tilde{\theta}_{opt} = \min [f_c(\theta)]$$

$$\tilde{p}_{opt} = p_m(I|\tilde{\theta}_{opt}) \tag{2}$$

In the above equations, $f_c(\theta)$ is the cost function, which is the absolute difference between two sand proportions: p_n is the sand proportion counted from the borehole logs; p_m is the sand proportion estimated

Table 1. Conversion of the Borehole Lithological Units to a Two Facies System Consisting of Sand and Clay^a

Symbol	Facies	Description
b	0	Well, hole bored in the earth
dg	2	Meltwater gravel, Glacial
di	1	Meltwater silt, Glacial
dl	1	Meltwater clay, Glacial
ds	2	Meltwater sand, Glacial
dv	0	Alternating thin meltwater beds, Glacial
dz	2	Meltwater stone, Glacial
g	2	Gravel and sand, unspecified
gi	1	Mica silt from Late Tertiary
gl	1	Mica clay from Late Tertiary
gp	1	Gyttja or coal, Late Tertiary
gs	2	Mica sand, Late Tertiary
i	1	Silt, unspecified
kg	2	Quartz gravel, Miocene
ks	2	Quartz sand, Miocene
l	1	Clay, unspecified
ll	1	Dense clay, Eocene
m	1	Mould, organic topsoil
mg	2	Gravel till, Glacial
ml	1	Clay till, Glacial
ms	2	Sand till, Glacial
o	1	Fill, man-made deposits
ol	1	Clay, Oligocene
p	1	Gyttja, organic mud, unspecified
s	2	Sand, unspecified
sl	1	Thick marl, Eocene
t	1	Peat, unspecified
ti	1	Freshwater silt, Late Glacial
u	0	Mixed clay sand and gravel, unspecified
v	0	Alternating thin beds, unspecified
x	0	Unknown bed
z	0	Stone, flint, unspecified

^a"1" indicates clay, "2" indicates sand, and "0" indicates the data that are not able to be classified, and therefore removed from the calculation.

from the AEM data, which depends on the cutoff value, θ . The optimized cutoff value ($\tilde{\theta}_{opt}$) is obtained at the place where the cost function reaches minimum, and thus the bias-adjusted sand proportion (\tilde{p}_{opt}) is the corresponding sand proportion calculated using the AEM data and the optimized cutoff value.

2.5. TProGS Modeling Package

TProGS was developed in order to simulate categorical variables through implementing transition probability and Markov Chain geostatistics. In TProGS, transition probability is used instead of the traditional variogram approach for categorical data due to its simplicity in formulating cross-correlated variables and interpreting the results. A two-category realization using TProGS is the same as using standard variogram-based geostatistics (e.g., SIS), since there is no asymmetry [Carle and Fogg, 1996]. There are three key steps involved in TProGS: first, the transition probabilities from observation data are established; second, Markov Chain (MC) models are developed in order to represent the spatial variability seen from the observed transition probability; third, Sequential Indicator Simulations (SIS) and quenching are applied so that the geological realizations are generated. The transition probability is defined as:

$$t_{j,k}(h) = \Pr \{k(x+h) | j(x)\} \quad (3)$$

where x is a location in space, h is the lag distance, j, k denotes two categories; it is possible that $j=k$. As seen from equation (3), transition probability can be interpreted as "the probability that facies k occurs at location $x+h$, given the condition that facies j occurs at location x " [Carle, 1996].

The 3-D MC models are generated to represent the spatial variability/dependency seen from the observed transition probability, where the mean length and the proportions of the facies are identified. MC assumes that the spatial occurrences depend only on the very nearest data, but not the data after that.

The 3-D MC model is then used as a reference in SIS and Quenching. In the SIS, first a random walking path is chosen for all the grid cells, which is different in each realization. Then along the randomly determined path, a grid is simulated by cokriging using values from the existing grids (both conditional data and already simulated grids). The simulation is carried out by assigning the grid category with respect to the probability distribution. The above process continues iteratively until all grids are filled. Next, Quenching is applied where the modeled grids generated with SIS are used as its initial configuration. The grids along the random path are then temporarily assigned to a different category as opposed to the SIS simulated category. An objective function is established to evaluate the statistical difference between the MC model from transition probability data and the MC model from the simulated realization. This iterative procedure proceeds until the objective function is optimized [Carle, 1996].

3. Results

Stochastic geological models are constructed for the TProGS model domain indicated in Figure 1. After delineating the glacial till sequence, only data inside the till area are used for histogram probability matching, for estimating transition probabilities and for conditional geological simulations. The simulation results,

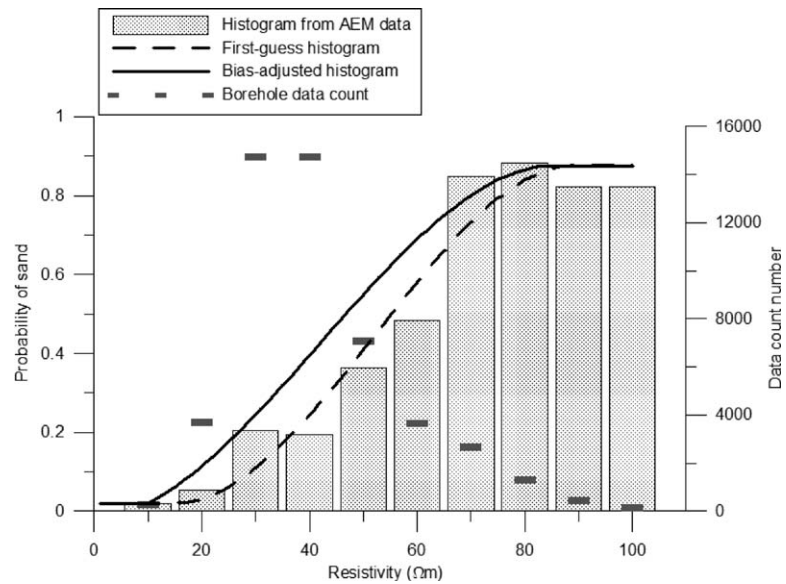


Figure 3. Histogram probability matching, including the bar chart developed using the observation data, the first-guess and the bias-adjusted histograms. The number of data pairs in each bin is indicated on the secondary vertical axis.

however, are generated and presented for the entire TProGS model domain in order to demonstrate the situations both with and without the influence of the conditioning data.

3.1. Histogram Probability Matching

Thirty-two different lithological units are identified in the geological borehole logs in the Norsminde area. Following the steps described in section 2.2, the lithological units are classified into a binary facies system consisting of only sand and clay. A list showing the results of this process can be seen in Table 1. The facies data are then discretized vertically into layers of 5 cm, which is the smallest scale at which sand units can be identified in the study area. Each of the 5 cm facies data is paired with the SkyTEM resistivity value from the corresponding 3-D grid. Since the interpolated AEM data have a vertical grid resolution of 2 m, up to 40 facies data are associated with one grid, assuming that the borehole data are not interrupted at that depth.

To link the resistivity spectrum to the facies, a histogram is established. It is decided to use 10 Ωm bin width to group the resistivity data, and in each bin the probability of sand is calculated as the number of logs categorized as sand divided by the total number of logs. In principle one can use either sand or clay to calculate the probability; however, since the purpose of the present study is to build geological models for ground-water simulation, sand is chosen because the highly conductive zones have a large impact on the transport. The higher end of the resistivity can reach values above 100 Ωm, but it rarely occurs in the Norsminde area. Therefore, the histogram ends at 100 Ωm which gives 10 bins in total. The histogram generated on borehole-SkyTEM data pairs is shown in Figure 3 as the bar chart. Once the histogram bars are determined, a third-order polynomial is used to perform curve fitting:

$$f(x) = \begin{cases} f_{\max}(x_2) & |x > x_2 \\ a \cdot x^3 + b \cdot x^2 + c \cdot x + d & |x_1 < x < x_2 \\ f_{\min}(x_1) & |x < x_1 \end{cases} \quad (4)$$

It should be mentioned that a third-order polynomial can be nonmonotonic, which is inconsistent with the concept of monotonically increasing probability of sand as resistivity increases (Figure 3). However, in the present case the function is confined when it reaches the maximum or minimum value at the two ends. This procedure ensures that higher resistivity values always indicate higher sand probability and vice versa. The histogram obtained by only fitting the observation data is referred to as the “first-guess histogram”

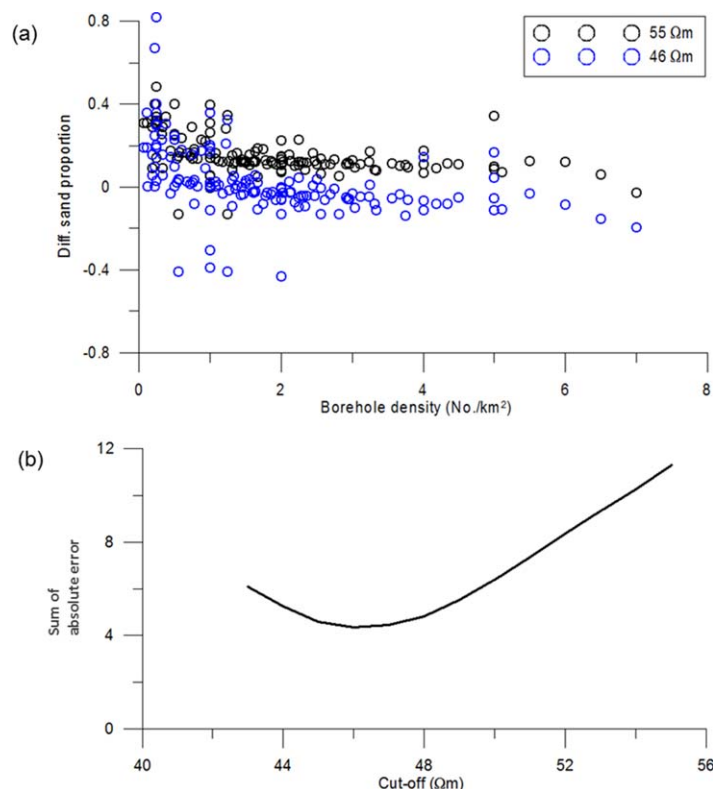


Figure 4. Identifying the cutoff value for the AEM data in order to separate sand and clay. (a) Differences of sand proportions between borehole data and AEM data using two cutoff values plotted against borehole density; and (b) sum of absolute error of sand proportions between the two types of data calculated for subareas with borehole density above 2/km² with varying cutoff values, equation(2).

(see Figure 3). The cutoff value to separate sand and clay which is read from the 50% sand probability is estimated to be 55 Ωm. Using this cutoff value, the sand proportion calculated from the AEM data is 12.1%, whereas the sand proportion calculated from borehole data is 29.4%. It is seen that the mismatch is substantial, and it is likely that the cutoff value is too high.

Various uncertainties affect the histogram resulting in a wide transition zone between the two facies, and thus the location of the cutoff value for separating sand and clay for the AEM data is also highly uncertain. However, in most geostatistical modeling tools, including TProGS, the proportion of a facies can only be given as a single value. Therefore, the mismatch in sand proportion between the two data types has to be resolved. In order to do so, equation (2) is applied to setup the cost function. It is assumed that the proportion mismatch is mainly caused by the unevenly

distributed sampling density of borehole data, meaning that the borehole data have insufficient representativeness at the locations where the borehole sampling frequency is low. Therefore, the disagreement in sand proportion is expected to be larger at the locations where borehole density is low, and to be in better agreement when the borehole density is higher than a certain threshold (thus more representative).

To address the borehole representativeness issue, the model domain is divided into 1 km² subdomains where the sand proportions are calculated individually. The subdomains with no boreholes are eliminated. The subdomains are then aggregated into larger subdomains (up until 81 km²) which give more combinations in terms of the sand proportion to borehole density relationship. The result of this analysis is shown in Figure 4a, where it can be roughly estimated that when the borehole density is larger than 2/km² the values fluctuate less. Therefore, the sum of absolute difference between the sand proportions of the two data types is only evaluated with borehole density above 2/km². This procedure is done iteratively with changing cutoff values from 43 to 55 Ωm. The result can be seen in Figure 4b, where the lowest cost function occurs at a cutoff value of 46 Ωm. The values behind Figure 4b are accumulated absolute errors for all subdomains that fulfill the borehole density threshold. For each subdomain, the probability of sand based on the AEM data is calculated using all grid values with no weighting, and the probability of sand based on borehole data is calculated using all available borehole data in that subdomain.

Using 46 Ωm as the cutoff value, the sand proportion calculated from the AEM data then becomes 23.7%, which will be used for the subsequent geostatistical analysis. As seen on Figure 4a the plot using 55 Ωm cutoff value indicates a positive bias (borehole minus AEM sand proportion), whereas the plot using 46 Ωm in general does not show obvious biases when the borehole density is above 2/km². Therefore, the 46 Ωm-to-50%-sand-probability is superimposed on the histogram by adding an extra point in curve fitting, where the polynomial is forced to go through this point. The resulting histogram, called “bias-adjusted histogram,” is shown in Figure 3. At this point, any resistivity value from the AEM data can be converted first to sand/

Table 2. Parameter Values Used in TProGS in Order to Establish Transition Probabilities Using the Observation Data on All Three Directions^a

	Lag (m)			Azimuth (°)		Dip (°)	
	Number	Spacing	Tolerance	Angle	Tolerance	Angle	Tolerance
Z	20 (10)	1(2)	0.5(1)	0	0	90	0
X	20	100	50	90	0	0	0
Y	20	100	50	0	0	0	0

^aNumbers in parentheses indicate the parameter values used for AEM data. If not specified, the same values are used for both borehole and AEM data.

clay facies based on the estimated cutoff value, and then associated with sand probability using the bias-adjusted histogram.

3.2. Transition Probability and Markov Chain Models

Observed transition probabilities are established using both borehole and AEM data, where the AEM resistivity data are converted to sand/clay facies using 46 Ωm as the cutoff value without considering the uncertainty. Borehole data are used without considering the quality rating.

A number of parameters needs to be specified in this process, see Table 2. The AEM data are measured exhaustively and provide abundant data in all directions. Borehole data sampling are less extensive in the horizontal direction but the data density is still sufficient for the analysis. Therefore, it is decided to use an angle tolerance of 0° for both azimuth and dip directions, which restricts the data search to directions aligned with the coordinate system of the geological model. Bandwidth, which is the maximum allowed distance perpendicular to the search angle, is therefore in this case irrelevant. The transition probability in the vertical direction is computed for a range of 20 m. Since the AEM data only exist every 2 m vertically, a lag spacing of 2 m is used; whereas for the borehole data, 1 m lag spacing is used. For the remaining parameters the same values are used for both data types.

Transiograms showing transition probabilities using the observation data are shown in Figure 5. The mean length is estimated by the interception of the first lag transition rate to the horizontal axis. In the vertical direction, transition probabilities calculated based on the two different data types are in good agreement. However, since the minimum lag distance of the AEM data is 2 m, the transition rates at small separations are different for the two data types: the mean length of sand is 5 m using the borehole data and 9 m using the AEM data. Therefore, in order to establish vertical transition rates more accurately, borehole data are indispensable, since a 2 m data interval from the AEM survey is relatively coarse and not able to resolve the natural length scale of sand.

In the horizontal direction, transiograms for both the X and Y directions were initially generated. However, they appear to be identical up to 1000 m, and the mean length estimated from X and Y directions are also identical. Therefore, the system is considered horizontally isotropic, and only the figure in 10 direction is displayed to avoid repetition. The first lag calculated using borehole data is completely offset: the AEM data suggest a mean length of sand of 500 m, whereas 1200 m is estimated from the borehole data. It is rather common to experience difficulty when estimating transition probability in the horizontal direction from borehole data alone according to previous studies [Weissmann and Fogg, 1999; Sakaki et al., 2009; Blessent et al., 2011]; however, the advantage introduced by high-resolution geophysical data is obvious, as the AEM data density is about 1000 time higher than the borehole density. Therefore, the two data types have their strengths and weaknesses in terms of identifying transition probability. It is also seen in Figure 5 that the observed data suggest different sand proportions, 23% and 30%, for AEM and borehole-based analysis, respectively. This is expected, because the sand proportion from the AEM data is obtained using the cost function as shown in section 3.1, whereas the sand proportion from the borehole data is obtained by point counting. Since it is only reasonable to have one Markov Chain model for the same system, the objective is not to make the two proportions match exactly, but to achieve a realistic sand proportion so that the MC modeling can be carried out.

TProGS offers a variety of options when choosing the method for 3-D Markov Chain modeling. It is also encouraged to integrate subjective knowledge in the modeling process [Fogg et al., 1998]. In the present study, it is chosen to use Embedded Markov Chain modeling, where clay is used as the background unit.

Therefore, the mean lengths of sand entered into the matrices are 5 and 500 m in vertical and horizontal directions, respectively. The modeled transition probability using the Embedded Markov Chain approach, Figure 5, successfully represents the observed data. Even though the transition rates at the first lag are not specified directly, the modeled transition probability fits the borehole data at the first lag in the vertical direction and AEM data in the horizontal direction.

3.3. Simulated Sand-Clay Texture Models

The borehole data are considered as the local truth in most studies. The present study provides an opportunity to introduce uncertainty on the borehole data through the quality rating exercise described in section 2.2. The result of the quality rating is shown in Table 3. The boreholes are classified into five quality groups from 1 to 5, where smaller number indicates higher quality. In stochastic geological simulations, borehole data are usually used as hard conditioning data, which means the probability given to the borehole data are 100%. In the present study, we use the borehole quality rating as a reference, and give probability scores to the borehole data based on which quality group they belong to. Therefore, quality group 1 is given a probability of 100%, same as hard conditioning, whereas the probability score decreases by 5% for subsequent quality groups (Table 3). This is considered a subjective way to incorporate uncertainty of borehole data as soft conditioning information.

Three conditioning scenarios are considered when generating the equally likely stochastic realizations using the modeled transition probabilities determined in the above section: (1) borehole data used as hard data, (2) borehole data used as soft data, and (3) both AEM and borehole data used as soft data. Each scenario is simulated with an ensemble of 10 realizations. The output cell size is 20 m × 20 m × 2 m, which is selected in order to resolve the geological features and also to make sure there is conditioning data in most grid cells. The horizontal extent of the simulation domain can be seen in Figure 1. Vertically 40 layers are generated using 21 m above sea level as the bottom of the model domain. The domain size and grid size are the same for all three scenarios. A 3-D illustration using realization 2 from scenario 1 is shown in Figure 6 together with the location of the boreholes. Horizontal slices at 49 m (above sea level) from realization 2, 4,

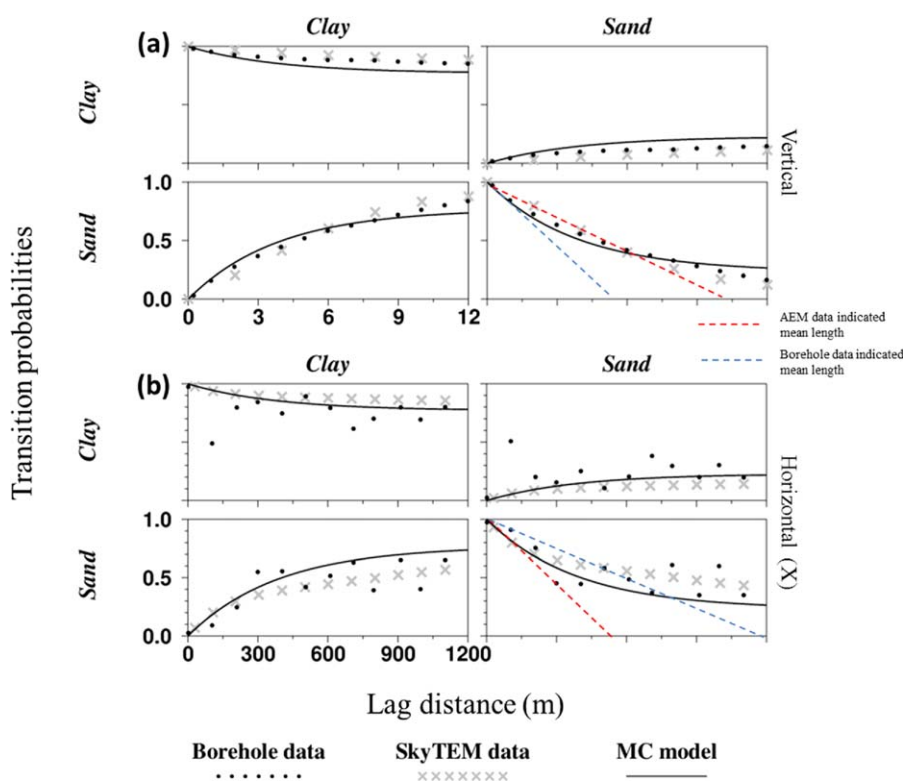


Figure 5. Transiograms for observed transition probability using borehole data and SkyTEM data, as well as modeled transition probability using Embedded Markov Chain model. (a) Vertical direction; and (b) horizontal direction.

Table 3. Rating of Borehole Data Quality in the Glacial Till Unit of the Norsminde Catchment

Quality Group	Number of Boreholes	Short Description	Probability for Conditioning (%)
1	25	High data sampling frequency, coordinates and level measured with differential GPS, trusted contractor and high-quality drilling method	100
2	34	Typically normal sampling frequency, trusted contractor and drilling method but without differential GPS measurements	95
3	43	Typically normal sampling frequency, poor drilling method and samples	90
4	10	Low data sampling frequency, very poor drilling method and samples	85
5	65	Very low quality, no data	

6, 8, and 10 for all three scenarios are illustrated in Figure 7. As seen in Figure 2, the horizontal coverage of the AEM conditioning data is not the same at different elevations. 49 m is chosen because it is one of the elevations where the largest lateral coverage of AEM data can be found, and also because it has a distinctive high resistivity cluster in the western part.

Figure 7 indicates that the degree of spatial variability between scenarios and between realizations in each scenario is very different. The borehole data-based scenarios 1 and 2 are similar, whereas the AEM data-based scenario 3 appears to be very different compared to the borehole-based scenarios: the location of sand lenses are much more fixed in scenario 3. This implies that the exhaustive AEM data set has a significant impact on reducing the uncertainty/spatial variation in conditional geological simulation. Since the SIS algorithm only considers the simulated Markov Chain model, which depends on the mean length of sand, the realizations based on borehole data conditioning show similar sizes of sand units on each realization, whereas the realizations based on the AEM data show a few large sand units and numerous scattered small ones. This is produced by TProGS to ensure the simulated mean length is statistically correct. The greater lateral continuity of sand bodies seen from the AEM-based models suggests that the conditioning data overwrite the mean length of sand obtained from the Markov Chain model.

It should be noted that the conditioning data are only used inside the glacial till structure. Areas where AEM data exist are highlighted in Figure 7. Both the spatial variability and the scale of the sand units are comparable for all three scenarios outside the highlighted area, where no conditioning data are applied. It is not possible to simulate an irregular shaped area with TProGS; therefore, the global sand proportion of 23.7% on the Markov Chain model may not apply to the subdomain of the glacial till area. In fact, based on the 10 realizations, the sand proportions inside the glacial till sequence are estimated to 21%, 25%, and 34% for scenarios 1, 2, and 3, respectively. When looking at the entire TProGS domain, the averaged sand proportions are the same for all three scenarios. This is controlled by the Markov Chain model. However, for the subdomain where the AEM data exist, the simulation results in artificially high values of sand proportion. This could be seen as a sign of strong conditioning. Moreover, the large discrepancies between the

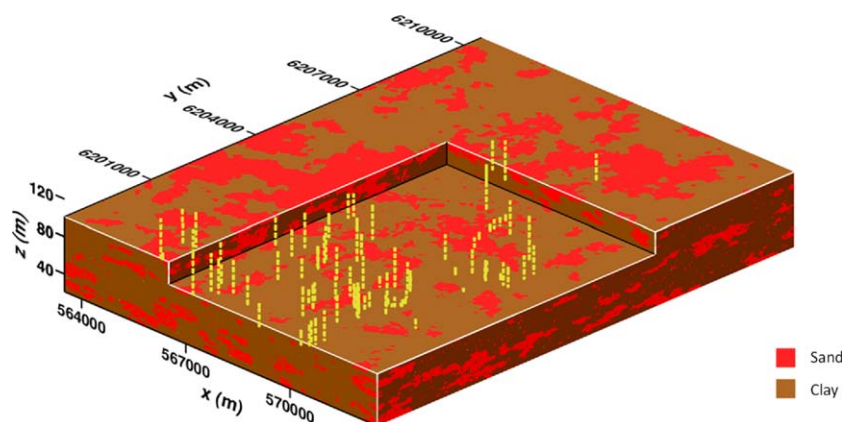


Figure 6. 3-D illustration of a TProGS realization together with the locations of the borehole data used for conditioning.

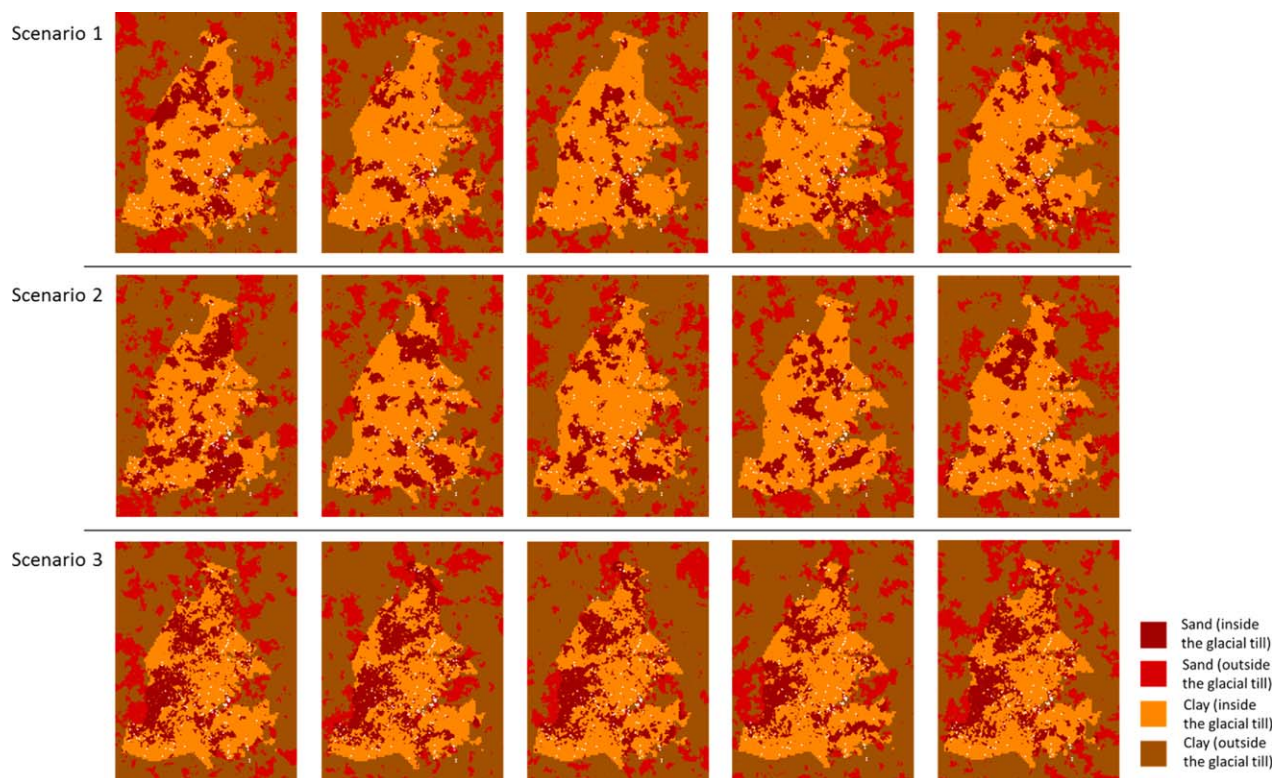


Figure 7. Simulated geological models using TProGS, horizontal slices are taken at 49 m above sea level. Borehole locations are also indicated by light yellow points. Three scenarios are presented: (1) using borehole data for hard conditioning, (2) using borehole data for soft conditioning; and (3) using both borehole and AEM data for soft conditioning. Five realizations are shown for each scenario.

simulated sand spatial distributions using borehole and SkyTEM data separately for conditioning implies that the system may not be stationary.

All in all, the above results show that when borehole data are used for conditional simulation, the geostatistical features, such as mean length and proportion of sand, are honored statistically better than when AEM data are used for data conditioning in the focus area. This shows that the selection of conditioning method is important for transition probability-based geostatistical simulations, and using a large number of data points for soft conditioning can effectively change the geostatistical features specified in TProGS.

4. Discussion

Our results have revealed new challenges when transforming airborne geophysical data to hydrogeological facies data, and subsequently using such data for establishing transition probabilities and carrying out stochastic geological simulation with soft data conditioning. The primary challenge when using the HPMM transformed data is that different sand proportions are found from the two different types of data (borehole and AEM). Since only one proportion can be specified for the Markov Chain model, the proportion mismatch is important to be addressed. Second, the borehole data have traditionally been considered as ground truth when the two types of data are compared. However, it is important to know what role the borehole data uncertainty plays during the data transformation. Last, the impact of conditioning data on the resulting geological models is analyzed.

4.1. Proportion Mismatch

We have proposed to use a histogram probability matching method to associate geophysical sounding data with borehole facies data. However, the cutoff value for the geophysical data is difficult to determine, and therefore causes proportion mismatch for the classified facies between the two data types. The cutoff

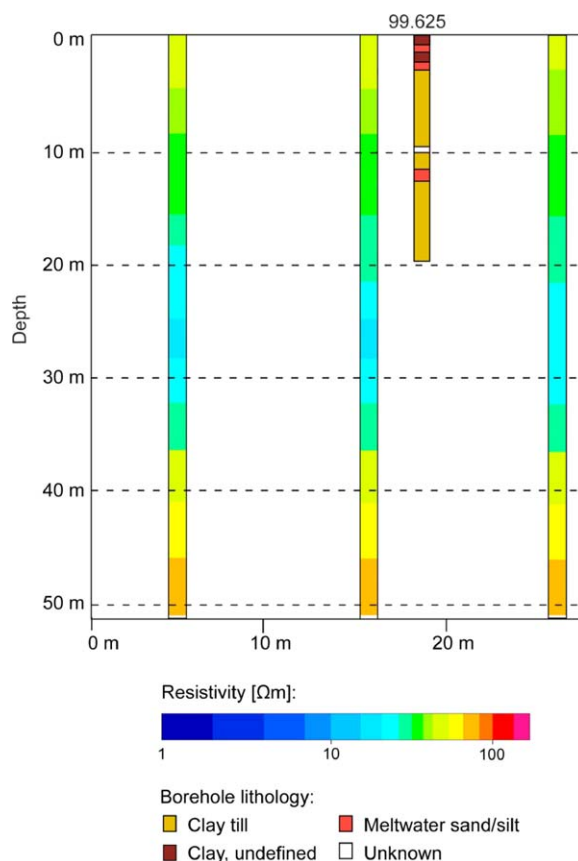


Figure 8. Side-by-side comparison of borehole lithological data and AEM vertical sounding data at borehole number 99.625.

units are not detected. In a conceptual three-layer model, when the resistivity value of the middle layer is much larger than the two neighboring layers, the electric current will tend to avoid the high resistivity sand layer and take the short route to the more conductive layer underneath. An example is shown in Figure 8 where the thin sand layer at depth 11–12 m is buried within a thick clay layer and therefore not identified by AEM. This phenomenon is amplified when the thickness of the resistive layer is small compared to its depth, and it is called “the principle of suppression” [Parasnis, 1997]. Based on this theory, the AEM data is expected to underestimate the volume of the sand units in areas where clayey (low resistive) sediments dominate. This is consistent with our observation.

On the other hand, the borehole data are likely to overestimate the sand proportion, which is mostly due to sampling bias [Proce et al., 2004]. First, boreholes are drilled at the places where high-permeable layers are assumed to exist based on previous knowledge, since the purpose for the majority of drillings in Denmark is to find groundwater aquifers. This can be seen in Figure 2 where the number of boreholes is unevenly distributed across the study area. Second, most drillings stop when a sandy aquifer is found. As a result, the clay sediments underneath the sand are not detected which also leads to overestimation of sand from the borehole log data [Nilsson et al., 2007]. However, in the present study, the second explanation does not apply. In fact, a large sand layer is present between the bottom of the glacial deposits and the top of the Miocene deposits, and most boreholes penetrate through both deposits. Since only the glacial deposits are studied and the boundary between the two layers is subjectively delineated, the location of the boundary can introduce uncertainty. If the boundary is shifted a few meters upward or downward, the sand proportion of the two facies changes significantly, as shown in Table 4.

Therefore, the AEM underestimation and the borehole overestimation imply that the sand proportion is neither 12.1% nor 29.4% seen from the first-guess histogram, but rather somewhere in between. The study uses an empirical search method to assess the “optimal” sand proportion. The estimated value of 23.7% for

value is initially estimated from the first-guess histogram where the resistivity value corresponding to 50% sand probability is found. However, this approach leads to large discrepancy of sand proportion between the two types of data. This indicates that the linkage between borehole facies data and AEM resistivity is uncertain. Figure 3 shows that the transition zone between high probability of sand and high probability of clay is quite wide. If 70% probability is taken for both facies, the transition zone is located between 43 and 68 Ωm . It is most likely that the “true” cutoff value is located somewhere within this range, but it is difficult to identify the exact location.

The proportion mismatch could be caused by both the geophysical data and the borehole data. The geophysical data have a tendency to underestimate sand units. AEM data normally show local-scale representativeness errors, because the small sand

Table 4. Proportion of Sand Estimated From Borehole Data and AEM Data With Alternative Bottom Elevation of the Glacial Till Structure (Unit: %)

Changed By	Borehole		SkyTEM	
	All Grades	Grade 1 Only	55 Ω m cutoff	46 Ω m cutoff
+ 10 m	18.4	22.1	4.4	11.7
+ 5 m	23.1	25.7	6.4	15.7
0 m	29.4	30.7	12.1	23.7
- 5 m	35.0	33.3	18.9	31.2
- 10 m	39.3	34.7	25.0	37.4

the entire area seems reasonable based on the results from the transition probability analysis. The bias-adjusted cutoff value, 46 Ω m, is also consistent with the resistivity ranges considered in C. Schamper et al. (submitted manuscript, 2013), where clay is characterized by resistivities in the range 25–60 Ω m and sand is defined by resistivities above 50 Ω m. The resistivity overlapping between the two hydrogeological facies illustrates the uncertainty in the link between the resistivity values and the lithology characterization.

Figure 3 shows that the distribution of sample pairs over the resistivity spectrum is much inclined to the low resistivity region which is a result of the large proportion of clay in the area. Considering that the AEM data actually highlight the conductive units and are inverted on a logarithmic scale in order to reflect the dynamics of the diffusive transient EM, the fitted histogram generated using linear scale can also introduce uncertainty. Therefore, the first-guess histogram is plotted using a log-transformed domain in Figure 9. The distribution of borehole data pairs is close to a normal distribution. The cutoff value for 50% sand probability is in this case 57 Ω m which is similar to what can be obtained using the linear-scale first-guess histogram (55 Ω m). This exercise indicates that using the log-transformed resistivity data to construct the histogram does not have significant impact on the resistivity-facies relationship, and thus the procedure for bias adjustment is necessary.

The vertical sampling scale of the two types of data differs by a factor of 40, as indicated in section 3.1, which could also result in mismatch of sand proportions. To evaluate the impact of the footprint difference, the borehole data are aggregated to 2 m intervals in order to match the AEM data footprint. The upscaling is done using the following procedure: borehole data are counted vertically using the 5 cm interval data set. An upscaling threshold is selected to classify the upscaled facies in every 2 m interval. For instance, if 60% upscaling threshold is chosen, it means that when the sand count within a 2 m interval suggests more than 60% is sand, then the whole 2 m is categorized as sand for the upscaled facies. After the 5 cm data set

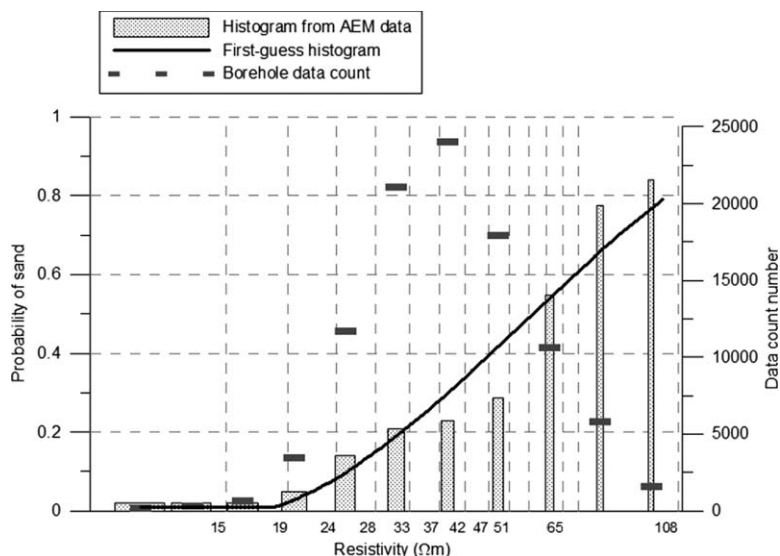


Figure 9. Histogram probability matching presented on log scale.

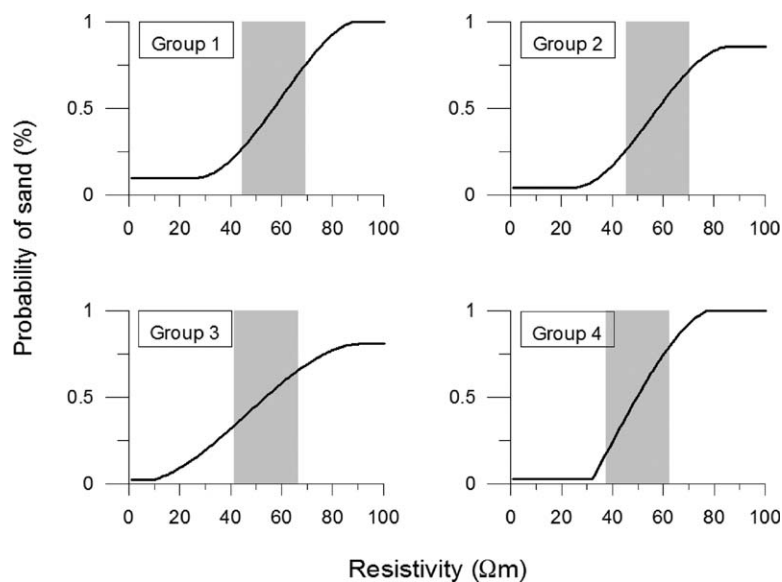


Figure 10. Histograms presented for different borehole quality ratings. The gray areas indicate the transition zones and are therefore excluded when calculating RMSEs.

is scanned, the sand proportion can be calculated for the 2 m rescaled data set. The objective is to match the original sand proportion by adjusting the upscaling threshold.

A trial-and-error approach is used to find the upscaling threshold, and the results can be seen in Table 5. It is noted that the upscaling thresholds can be adjusted such that the sand proportion of the fine-resolution data sets is successfully matched. The value of the upscaling threshold indicates the impact of sampling scale on the estimated proportion. If all four quality groups are considered, the upscaling threshold is 50% indicating that a sampling scale of 2 m using the dominant facies (the one above 50%) will give similar results to using a sampling scale of 5 cm. This is logical because the 2 m sampling scale is significantly smaller than the vertical mean length scale of 5 m (Figure 5). This implies that if the histogram was constructed using the 2 m interval data, the histogram would not show a significantly different shape. However, it is still preferable to use the 5 cm data to identify the mean length as stated in section 3.2.

The difference in the mean length of sand in vertical direction obtained from borehole and AEM data, 5 and 9 m, respectively (Figure 5), indicates that the measurement footprint of the AEM data is larger than the 2 m resolution of the data set. Thus, the volume of soil over which the electric currents propagate in the soil and the additional smoothing of the data caused by the numerical inversion algorithm limit the effective vertical resolution of the information suggesting that the AEM system may have difficulty identifying a sand unit with a vertical extent of 2 m. The vertical resolution of the AEM data also has an effect on the results in the horizontal direction. Since the AEM data are averaged across a 2 m deep interval, the same 2 m averaging is occurring across the entire voxel that is used for the horizontal measure, which will affect both the proportion and the mean length. This addresses the importance of the resolution of a device: borehole data

are well resolved in both horizontal and vertical directions; however, the borehole data are also extremely sparse in the horizontal direction. AEM data, on the other hand, have a much coarser resolution; however, these data are very dense in the horizontal direction.

Table 5. Proportion of Sand With Borehole Data Rescaled From 5 to 2 m (Unit: %)^a

Quality Group	Sand Proportion in 5 cm Vertical Depth	Sand Proportion in 2 m Rescale	Upscaling Threshold
1	30.7	30.7	48
2	25.2	25.5	52
3	34.6	34.3	50
4	21.6	21.8	61
All (1–4)	29.4	29.4	50

^aQuality groups are defined in Table 3.

4.2. Impact of Borehole Quality

When comparing borehole data and the AEM data in the histogram probability

matching method, borehole data are considered as the true representation of the hydrogeological facies. However, the shape of the fitted histogram, especially the width of the transition zone, indicates that uncertainties from various sources are lumped into the data. These uncertainties include: first, borehole descriptions are not accurate, and classification of borehole lithology is subjective. Second, there are uncertainties on the resistivity data due to the resolution of the physics itself, the geophysics instruments, field measurements and signal processing (inversion). Third, there is no unique relationship between resistivity and lithology, and the curve can therefore be fitted in various ways. Last, there are uncertainties related to the scale of aggregation, since the borehole data and geophysical data have different resolutions and hence different supporting scales [Refsgaard *et al.*, 2014]. The difference between the actual histogram and the “ideal” histogram (where only zeros exist below the cutoff value and ones above the cutoff value) indicates the magnitude of the combined uncertainty. It also means that the larger the combined uncertainty, the lower the slope of the fitted histogram will get.

It can be useful to acknowledge the borehole quality rating information and examine the influence that the borehole data quality plays in generating the histogram. In order to do so, the following steps are taken: first, individual first-guess histograms are prepared for each borehole quality group. Second, cutoff values that separate clay and nonclay are identified. Last, root-mean-square errors (RMSEs) are calculated for each histogram comparing to the ideal histograms, while excluding data $\pm 10 \Omega\text{m}$ from the cutoff values. The results are shown in Figure 10 and the corresponding statistics are listed in Table 6.

If the uncertainty from the borehole data is the dominating uncertainty, decreasing slope should be observed with decreasing borehole quality. However, this trend is not entirely clear in Figure 10. The slope is found to decrease from quality groups 1 to 3; however, quality group 4 seems to have highest slope and hence the best performance. Comparing the RMSE values in Table 6, the same conclusion can be obtained. It seems that the relatively good match obtained between the borehole data and the AEM data in group 4 is not caused by high data quality but related to the frequency of facies shift per 10 m. If other factors are equal, the higher the borehole quality, the more heterogeneity they are able to represent. As a result, the better match between the borehole data and AEM data can be a coincidence due to the fact that both data types have smoothed facies transition. Additionally, there are only 10 boreholes in group 4, and the sample volume might be too small to be representative. Therefore, it is inconclusive whether borehole data uncertainty has the dominating effect to the overall uncertainty.

4.3. Impact of the Conditioning Strategy

One of the main objectives of the present study is to evaluate if and how exhaustively sampled grid-to-grid airborne geophysical data can be used in geostatistical simulations. This is implemented through incorporating AEM data as soft information for constraining SIS in TProGS. The simulated results suggest considerable differences compared to the scenario where only the borehole data are used. In order to analyze the impact of the conditioning data on estimates of facies uncertainty at point locations, the probability of sand for each pixel is calculated based on the 10 realizations. This is done for all three scenarios at the elevation of 31, 49, and 59 m. and the results are shown in Figure 11. The simulated probability of sand is an indication of the variability between realizations. Using borehole data as soft information (Figure 11c) results in higher variability than if the borehole data are used for hard conditioning (Figure 11b) as expected. It is noted that the quality scores for different borehole groups (seen in Table 3) are subjective. Thus, if lower scores are used, the difference between scenario 1 and 2 will be larger. However, the difference between scenario 1 and 2 is small compared to the difference between scenario 2 and 3, when AEM data are added.

The AEM data-based simulations (Figure 11d) indicate almost deterministic results at the locations where conditioning data are available (Figure 11a) regardless of the depth. In the densely conditioned areas, the probability of sand or clay is above 80%. This is a clear indication that the simulations have been strongly conditioned in the horizontal direction. In order to quantitatively illustrate the strongly conditioned simulation results, cumulative density functions (CDF) are plotted against sand probabilities for all three simulation scenarios. It is seen in Figure 12a that the AEM transformed facies data, which is used for soft conditioning, aligns very well with the two simulation scenarios generated with borehole data as conditioning information (scenario 1 and 2). However, the AEM data-based simulations (scenario 3) show a flat shape of the CDF which indicates that the probability of sand has been magnified. Therefore, it is believed that the main reason for the difference between the AEM-based simulations and the borehole-based simulations is the

Table 6. Histogram Cutoff Values in Relation to Different Borehole Quality Groups^a

Quality Group	Number of Boreholes	Cutoff Value (Ω m)	RMSE	Point Counts	Number of Facies Shift (per 10 m)
1	25	57	0.17	8714	9.9
2	34	58	0.19	17,733	2.7
3	43	54	0.28	18,509	2.0
4	10	50	0.16	3892	0.6

^aQuality groups are defined in Table 3. The frequency of facies shift is calculated for every 10 m.

conditioning strategy, and because of that the geostatistical features (mean length and proportion) are not honored in the AEM-based simulations.

It is estimated that the mean length of sand in the horizontal direction is 500 m whereas the conditioning data is provided every 20 m and the output grid size is also 20 m. The AEM data are spatially correlated and it is speculated that TProGS has difficulties dealing with spatially correlated data. In the cokriging process of the current TProGS version, the uncertainty of the soft conditioning data are considered when randomly selecting the facies for interpolation, but the uncertainty is not considered when calculating the kriging covariance matrix. Therefore, this results in an artificial reduction of the uncertainty of the correlated data. Hydrological simulations using strongly conditioned realizations of the geology will show similar flow paths.

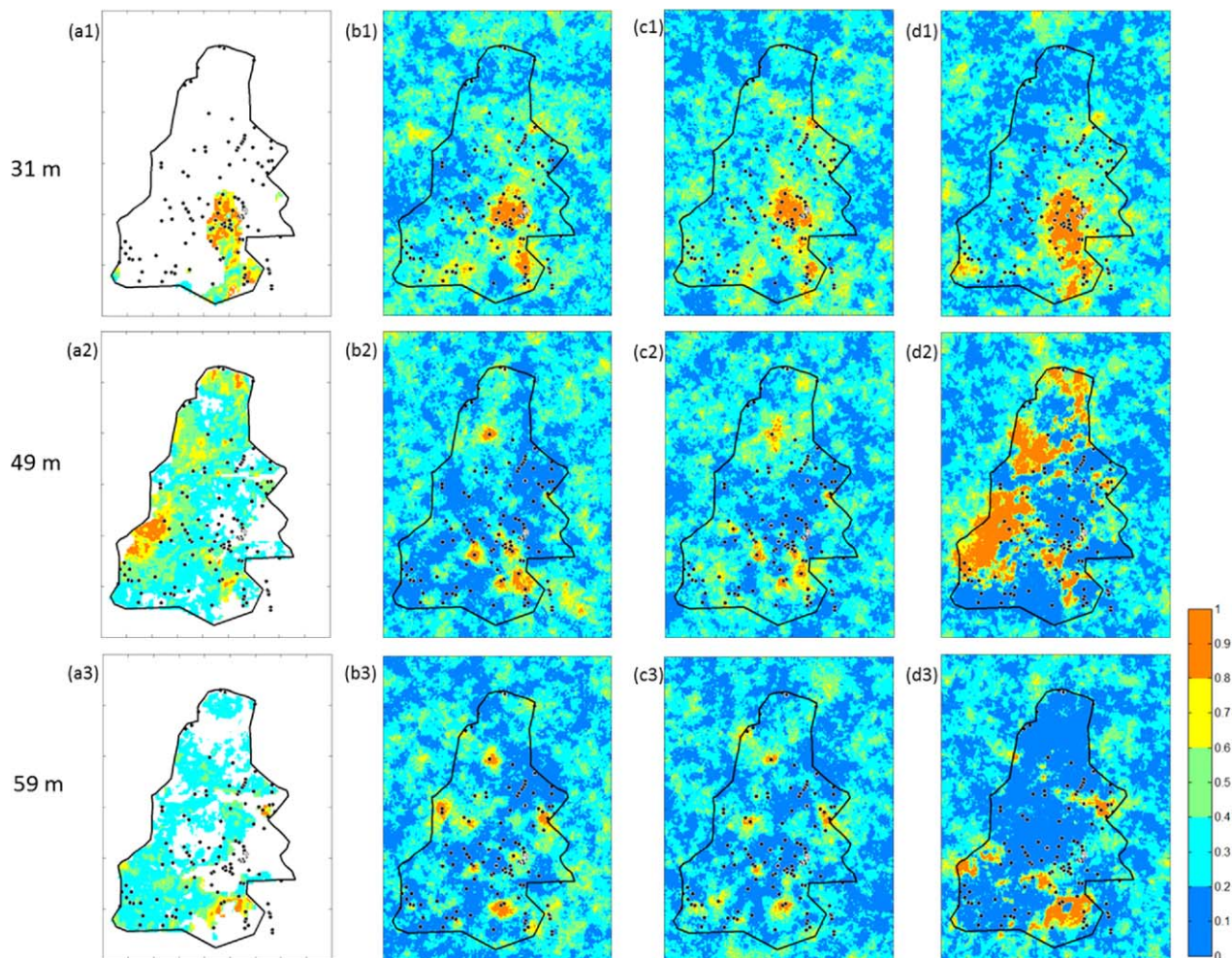


Figure 11. Simulated sand probabilities each based on 10 TProGS realizations at 31, 49, and 59 m above sea level. The locations of boreholes are indicated as black points. (a) Probability of sand for the transformed AEM data using HPMM, (b) using borehole data for hard conditioning, (c) using borehole data for soft conditioning, and (d) using both borehole data and AEM data for soft conditioning. Figure 11b–11d correspond to scenario 1–3 in Figure 7, respectively.

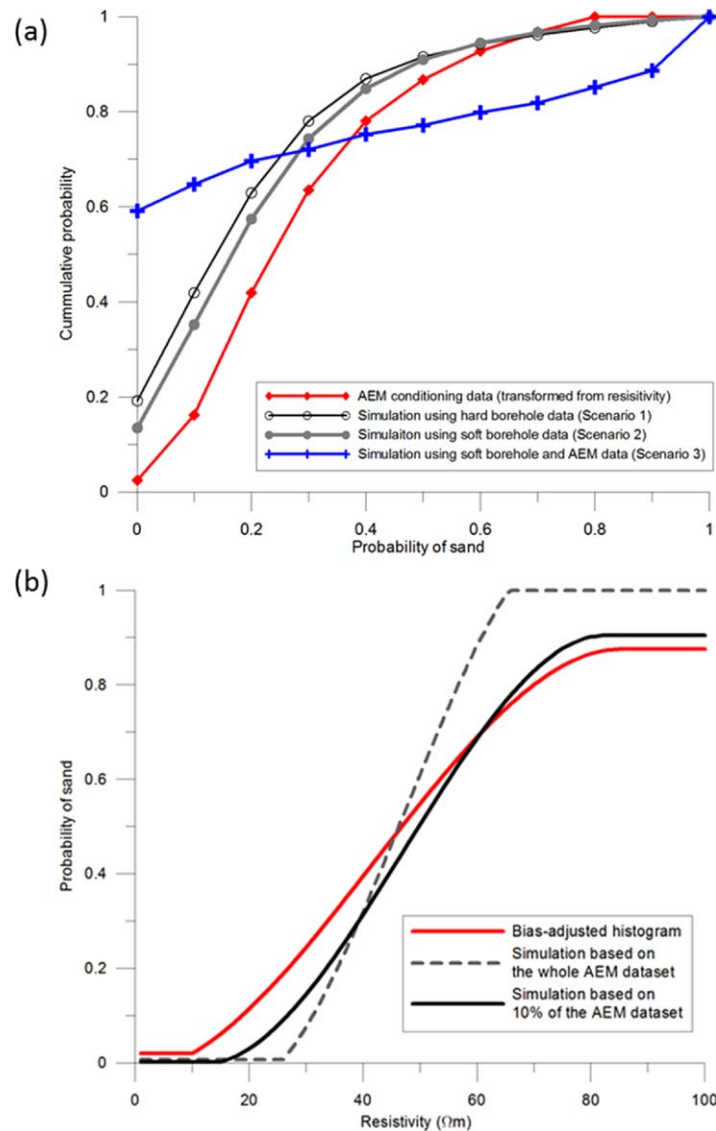


Figure 12. Illustration of simulation that is strongly conditioned by AEM data used as soft conditioning information. (a) Cumulative density functions (CDFs) plotted against probability of sand for the AEM conditioning data and three simulation scenarios as seen in Figure 7; and (b) reproducing the histogram using the simulation results with the whole AEM data set and reduced AEM data set.

Possible solutions for this problem might be: (1) thinning out the conditioning data so they are no longer correlated or less correlated; (2) adding uncertainty when producing the histogram to account for the data correlation; (3) update the cokriging function in TProGS so the data uncertainty can be considered when calculating the covariance matrix. Here the first method has been tested, where the amount of conditioning data is reduced by 90% and the simulations are reproduced. On the original AEM data set, every one out of ten data entry is kept using the same sampling spacing. The resulting resistivity-to-sand-probability relationship is compared with the bias-adjusted histogram and the simulation where the entire AEM data set is used for conditioning, Figure 12b. By removing the majority of the conditioning data, the estimated uncertainty is at the level which was originally intended (the same as the bias-adjusted histogram). However, further implementations and analysis for dealing with the correlated data are outside the scope of the present study.

It is shown in Figure 11 that for the three selected depths, the largest difference between the simulation scenarios occurs at 49 m elevation. At 49 m elevation, the largest difference between scenario 3 and scenario 1

appears to be on the south west corner of the study area, where the AEM-based simulations suggest very large probability of sand, whereas the borehole-based simulations suggest large probability of clay. This is because borehole data missed this large sand unit due to insufficient sampling. There is only one borehole reaching 49 m at the location where AEM data indicates sand. Based on this borehole alone, it is not possible to generate a sand unit with the same size as can be done using AEM data for conditioning. Therefore, the comprehensive AEM data have certain advantages in simulating the geology in the study area. The large sand unit at 49 m may be mapped based on borehole data for conditioning if a three-facies system was used, since many of the resistivity data in that area belongs to the transition zone. The reasons why it was decided to use a two facies system to begin with are: first, the borehole data have to be classified into a number of hydrogeological facies, so that they can be paired with resistivity data. The borehole lithological descriptions originally contained 32 units, as seen in Table 1. If the borehole data are classified into three hydrofacies (sand, clay, and an in-between facies), it is very difficult to determine which lithological units that belong to the intermediate facies. Second, as a first attempt to carry out such lithological-geophysical

data pairing, we would like to keep our experiment as simple as possible. If three facies are used, the histogram probability matching method will also have to involve cross relations between every two of the three facies.

Another way to demonstrate the influence of using abundant AEM data for geological simulation is a cross-validation analysis, which can be carried out by examining the effect of AEM data on the TProGS results using an independent data set. Since there is no independent data set available, we have therefore split the borehole data into two subgroups with equal population using random selection: one for conditioning the TProGS simulations and the other for validating the results. The voxel values from TProGS are compared to the collocated borehole data. For scenario 2 (borehole data used for soft conditioning) 32.6% agreement with validation data is found in terms of simulating the sand units at the correct location, whereas the agreement is 77.2% for scenario 3 (both borehole and AEM data used for conditioning). The improvement caused by adding the geophysical data into the conditional simulation process is obvious. It shows that using both AEM and borehole data is superior for finding the correct locations of sand lenses compared to the case where borehole data is the only data source for conditioning.

2-D or 3-D geophysical data have been used in geostatistical techniques such as indicator geostatistics, multiple-point geostatistics and object-based methods [Deutsch and Wen, 2000; Parra et al., 2006; Mariethoz et al., 2009; Engdahl et al., 2010b]. However, employing AEM data for stochastic hydrofacies simulation is a relatively new field where only a few studies have been published. Therefore, the results presented in the present study have certain novelties in this particular subject. As far as we know, only Gunnink and Siemon [2009] and He et al. [2013] have tried to use AEM data for stochastic geological simulations. The geophysical data employed by Gunnink and Siemon [2009] were based on frequency EM (FEM). The current study uses transient EM (TEM) which usually has a lower resolution close to the ground surface than FEM. However, since the TEM version we used (SkyTEM101) has been optimized for higher-resolution near surface (C. Schamper et al., submitted manuscript, 2013), the airborne geophysical data used in the two studies are in fact comparable regarding near-surface resolution, and thus the results are also similar in terms of the sand-clay texture models. On the other hand, He et al. [2013] used the conventional TEM technology and the flight line spacing was twice as high compared to the present study. The geology in their study area was described as a glaciotectionic complex which means that the degree of geological heterogeneity is higher and the correlation length is smaller than in the glacial till sequence. They later found that the correlation length of their system was significantly smaller than what was resolved in the geological model based on the TEM data, and therefore it was difficult to identify the correlation length properly. This indicates that the AEM data density plays an important role depending on the specific geological condition.

5. Summary and Conclusions

In the present study, the geostatistical modeling tool TProGS is used to simulate structures of sand/clay-dominated glacial deposits. The simulations use in situ borehole data and airborne geophysical data for establishing transition probabilities as well as for conditioning the stochastic indicator simulations. The exhaustive geophysical data are used with consideration of their uncertainties, which is an innovative contribution of the study. To our knowledge, it is also the first time that TProGS is applied in conditional simulations with such extensive geophysical data.

A histogram probability matching method is used to associate the resistivity data from the AEM survey to facies categories. The resulting first-guess histogram shows large discrepancies in terms of sand proportions from the AEM data compared to the results using borehole data (12.1% and 29.4%, respectively). This mismatch indicates that the linkage between these two types of data is highly uncertain which is shown as a wide transition zone from clay to sand on the fitted histogram.

The wide transition zone is attributed to various reasons such as data uncertainty, the curve fitting method and the footprint of measurement. An empirical cost function is therefore used to assess an optimal sand proportion. The bias-adjusted cutoff value of 46 Ωm is obtained for dividing sand and clay; and the corresponding sand proportion is 23.7%. It is later shown that by using the cutoff value from the empirical method, the resulting transition probabilities are reasonable. However, the simulated spatial patterns based on AEM data show very large differences when compared to the borehole data-based simulations. Moreover, it is also indicated that the selection of log-transformed resistivity data for generating the histogram

did not play a significant role, but the delineation of the target area (the glacial till sequence) has an important impact.

The transition probabilities established from the two types of observation data are in good agreement in both vertical and horizontal directions when the bias-adjusted cutoff value is used. The estimated mean lengths of sand units are 5 m vertically and 500 m horizontally for the Quaternary glacial till deposits. The geological heterogeneity as well as connectivity can also be well represented by TProGS. Because of the high data density, the AEM data are superior in horizontal directions, whereas borehole data are favorable in the vertical direction for identifying observed transition probabilities. Additionally, TProGS has shown the ability to combine the information from different sources of data in different directions.

The results show that the selection of conditioning method is critical for transition probability-based geostatistical simulations: when borehole data are used, the assigned spatial statistics are better honored, whereas when AEM data are used, the simulations tend to follow the conditioning information and leave very little room for variability between realizations. Meanwhile, the AEM data are indispensable for simulating sand units when there is a lack of borehole data coverage. The cross-validation analysis shows a large improvement when AEM is introduced compared to the case where borehole data are used alone. However, the strongly conditioned simulation results caused by abundant AEM data and the data uncertainty problem are not yet fully accounted for.

Acknowledgments

This work has been a part of the NiCA (Nitrate Reduction in a Geologically Heterogeneous Catchment) project, which is funded by the Danish Council for Strategic Research. Claus Ditlefsen is thanked for his input and help in the development of the borehole rating system. We would like to thank Dylan Harp, Gary Weissmann, and one anonymous reviewer for their helpful comments during the review process.

References

- Auken, E., A. V. Christiansen, J. H. Westergaard, C. Kirkegaard, N. Foged, and A. Viezzoli (2009), An integrated processing scheme for high-resolution airborne electromagnetic surveys, the SkyTEM system, *Explor. Geophys.*, *40*(2), 184–192.
- Berkowitz, B. (2002), Characterizing flow and transport in fractured geological media: A review, *Adv. Water Resour.*, *25*(8–12), 861–884.
- Blessent, D., R. Therrien, and J. M. Lemieux (2011), Inverse modeling of hydraulic tests in fractured crystalline rock based on a transition probability geostatistical approach, *Water Resour. Res.*, *47*, W12530, doi:10.1029/2011WR011037.
- Carle, S. F. (1996), T-PROGS: Transition probability geostatistical software, report, Univ. of Calif., Davis.
- Carle, S. F. (1997), Implementation schemes for avoiding artifact discontinuities in simulated annealing, *Math. Geol.*, *29*(2), 231–244.
- Carle, S. F., and G. E. Fogg (1996), Transition probability-based indicator geostatistics, *Math. Geol.*, *28*(4), 453–476.
- Carle, S. F., B. K. Esser, and J. E. Moran (2006), High-resolution simulation of basin-scale nitrate transport considering aquifer system heterogeneity, *Geosphere*, *2*(4), 195–209.
- Christiansen, A. V., and N. B. Christensen (2003), A quantitative appraisal of airborne and ground-based transient electromagnetic (TEM) measurements in denmark, *Geophysics*, *68*(2), 523–534.
- Christiansen, A. V., E. Auken, and K. I. Sørensen (2006), *The Transient Electromagnetic Method*, Springer, Berlin, Germany.
- de Almeida, J. A. (2010), Stochastic simulation methods for characterization of lithoclasses in carbonate reservoirs, *Earth Sci. Rev.*, *101*(3–4), 250–270.
- De Benedetto, D., A. Castrignano, D. Sollitto, F. Modugno, G. Buttafuoco, and G. lo Papa (2012), Integrating geophysical and geostatistical techniques to map the spatial variation of clay, *Geoderma*, *171*, 53–63.
- dell'Arciprete, D., R. Bersezio, F. Felletti, M. Giudici, A. Comunian, and P. Renard (2012), Comparison of three geostatistical methods for hydrofacies simulation: A test on alluvial sediments, *Hydrogeol. J.*, *20*(2), 299–311.
- Deutsch, C. V., and P. W. Cockerham (1994), Practical considerations in the application of simulated annealing to stochastic simulation, *Math. Geol.*, *26*(1), 67–82.
- Deutsch, C. V., and X. H. Wen (2000), Integrating large-scale soft data by simulated annealing and probability constraints, *Math. Geol.*, *32*(1), 49–67.
- Elfeki, A. M. M. (2006), Reducing concentration uncertainty using the coupled Markov Chain approach, *J. Hydrol.*, *317*(1–2), 1–16.
- Elfeki, A. M. M., and F. M. Dekking (2007), Reducing geological uncertainty by conditioning on boreholes: The coupled Markov Chain approach, *Hydrogeol. J.*, *15*(8), 1439–1455.
- Engdahl, N. B., E. T. Vogler, and G. S. Weissmann (2010a), Evaluation of aquifer heterogeneity effects on river flow loss using a transition probability framework, *Water Resour. Res.*, *46*, W01506, doi:10.1029/2009WR007903.
- Engdahl, N. B., G. S. Weissmann, and N. D. Bonal (2010b), An integrated approach to shallow aquifer characterization: Combining geophysics and geostatistics, *Comput. Geosci.*, *14*(2), 217–229.
- Falivene, O., L. Cabrera, J. A. Munoz, P. Arbues, O. Fernandez, and A. Saez (2007), Statistical grid-based facies reconstruction and modelling for sedimentary bodies. Alluvial-palustrine and turbiditic examples, *Geol. Acta*, *5*(3), 199–230.
- Feyen, L., and J. Caers (2006), Quantifying geological uncertainty for flow and transport modeling in multi-modal heterogeneous formations, *Adv. Water Resour.*, *29*(6), 912–929.
- Fogg, G. E., C. D. Noyes, and S. F. Carle (1998), Geologically based model of heterogeneous hydraulic conductivity in an alluvial setting, *Hydrogeol. J.*, *6*(1), 131–143.
- Franssen, H. J. W. M. H., and J. J. Gomez-Hernandez (2002), 3D inverse modelling of groundwater flow at a fractured site using a stochastic continuum model with multiple statistical populations, *Stochastic Environ. Res. Risk Assess.*, *16*(2), 155–174.
- Goovaerts, P. (2001), Geostatistical modelling of uncertainty in soil science, *Geoderma*, *103*(1–2), 3–26.
- Gunnink, J., and B. Siemon (2009), Combining airborne electromagnetics and drilling to construct a stochastic 3D lithological model, paper presented at 15th European Meeting of Environmental and Engineering Geophysics, Dublin, Ireland, Houten, the Netherlands.
- Gunnink, J., J. H. A. Bosch, B. Siemon, B. Roth, and E. Auken (2012), Combining ground-based and airborne em through artificial neural networks for modelling glacial till under saline groundwater conditions, *Hydrol. Earth Syst. Sci.*, *16*(8), 3061–3074.
- Harp, D. R., Z. X. Dai, A. V. Wolfsberg, J. A. Vrugt, B. A. Robinson, and V. V. Vesselinov (2008), Aquifer structure identification using stochastic inversion, *Geophys. Res. Lett.*, *35*, L08404, doi:10.1029/2008GL033585.

- He, X., T. O. Sonnenborg, F. Jørgensen, A. S. Hoyer, R. R. Møller, and K. H. Jensen (2013), Analyzing the effects of geological and parameter uncertainty on prediction of groundwater head and travel time, *Hydrol. Earth Syst. Sci.*, *17*(8), 3245–3260.
- Henriksen, H. J., L. Trolborg, P. Nyegaard, T. O. Sonnenborg, J. C. Refsgaard, and B. Madsen (2003), Methodology for construction, calibration and validation of a national hydrological model for Denmark, *J. Hydrol.*, *280*(1–4), 52–71.
- Hill, M., and C. R. Tiedeman (2007), *Effective Groundwater Model Calibration*, John Wiley, Hoboken, N. Jersey.
- Hu, L. Y., and T. Chugunova (2008), Multiple-point geostatistics for modeling subsurface heterogeneity: A comprehensive review, *Water Resour. Res.*, *44*, W11413, doi:10.1029/2008WR006993.
- Højberg, A. L., and J. C. Refsgaard (2005), Model uncertainty—Parameter uncertainty versus conceptual models, *Water Sci. Technol.*, *52*(6), 177–186.
- James, B. R., and R. A. Freeze (1993), The worth of data in predicting aquitard continuity in hydrogeological design, *Water Resour. Res.*, *29*(7), 2049–2065.
- Jørgensen, F., and P. B. E. Sandersen (2006), Buried and open tunnel valleys in Denmark—Erosion beneath multiple ice sheets, *Quat. Sci. Rev.*, *25*(11–12), 1339–1363.
- Jørgensen, F., et al. (2012), Transboundary geophysical mapping of geological elements and salinity distribution critical for the assessment of future sea water intrusion in response to sea level rise, *Hydrol. Earth Syst. Sci.*, *16*(7), 1845–1862.
- Jørgensen, F., R. R. Møller, L. Nebel, N.-P. Jensen, A. V. Christiansen, and P. B. E. Sandersen (2013), A method for cognitive 3D geological voxel modelling of AEM data, *Bull. Eng. Geol. Environ.*, *72*(3), 421–432.
- Juang, K. W., Y. S. Chen, and D. Y. Lee (2004), Using sequential indicator simulation to assess the uncertainty of delineating heavy-metal contaminated soils, *Environ. Pollut.*, *127*(2), 229–238.
- Kirkegaard, C., T. O. Sonnenborg, E. Auken, and F. Jørgensen (2011), Salinity distribution in heterogeneous coastal aquifers mapped by airborne electromagnetics, *Vadose Zone J.*, *10*(1), 125–135.
- Kollet, S. J., and R. M. Maxwell (2006), Integrated surface-groundwater flow modeling: A free-surface overland flow boundary condition in a parallel groundwater flow model, *Adv. Water Resour.*, *29*(7), 945–958.
- Lee, S. Y., S. F. Carle, and G. E. Fogg (2007), Geologic heterogeneity and a comparison of two geostatistical models: Sequential gaussian and transition probability-based geostatistical simulation, *Adv. Water Resour.*, *30*(9), 1914–1932.
- Lemieux, J. M., E. A. Sudicky, W. R. Peltier, and L. Tarasov (2008), Dynamics of groundwater recharge and seepage over the canadian landscape during the wisconsinian glaciation, *J. Geophys. Res.*, *113*, F01011, doi:10.1029/2007JF000838.
- Mariethoz, G., P. Renard, and R. Froidevaux (2009), Integrating collocated auxiliary parameters in geostatistical simulations using joint probability distributions and probability aggregation, *Water Resour. Res.*, *45*, W08421, doi:10.1029/2008WR007408.
- McKenna, S. A., and E. P. Poeter (1995), Field example of data fusion in site characterization, *Water Resour. Res.*, *31*(12), 3229–3240.
- McLaughlin, D., L. B. Reid, S. G. Li, and J. Hyman (1993), A stochastic method for characterizing groundwater contamination, *Ground Water*, *31*(2), 237–249.
- Nilsson, B., A. L. Højberg, J. C. Refsgaard, and L. Trolborg (2007), Uncertainty in geological and hydrogeological data, *Hydrol. Earth Syst. Sci.*, *11*(5), 1551–1561.
- Parasnis, D. S. (1997), *Principles of Applied Geophysics*, Springer, Berlin, Germany.
- Parra, J. O., C. L. Hackert, and M. W. Bennett (2006), Permeability and porosity images based on p-wave surface seismic data: Application to a south florida aquifer, *Water Resour. Res.*, *42*, W02415, doi:10.1029/2005WR004114.
- Poeter, E., and D. Anderson (2005), Multimodel ranking and inference in ground water modeling, *Ground Water*, *43*(4), 597–605.
- Proce, C. J., R. W. Ritzi, D. F. Dominic, and Z. X. Dai (2004), Modeling multiscale heterogeneity and aquifer interconnectivity, *Ground Water*, *42*(5), 658–670.
- Quental, P., J. A. Almeida, and M. Simoes (2012), Construction of high-resolution stochastic geological models and optimal upscaling to a simplified layer-type hydrogeological model, *Adv. Water Resour.*, *39*, 18–32.
- Rasmussen, E. S., K. Dybkjaer, and S. Piasecki (2010), Lithostratigraphy of the upper oligocene—Miocene succession of Denmark, *Geol. Surv. Den. Greenl. Bull.*, *22*, 5–13.
- Refsgaard, J. C., J. P. van der Sluijs, J. Brown, and P. van der Keur (2006), A framework for dealing with uncertainty due to model structure error, *Adv. Water Resour.*, *29*(11), 1586–1597.
- Refsgaard, J. C., S. Christensen, T. O. Sonnenborg, D. Seifert, A. L. Højberg, and L. Trolborg (2012), Review of strategies for handling geological uncertainty in groundwater flow and transport modeling, *Adv. Water Resour.*, *36*, 36–50.
- Refsgaard, J. C., et al. (2014), Nitrate reduction in geologically heterogeneous catchments—A framework for assessing the scale of predictive capability of hydrological models, *Sci. Total Environ.*, *468–469*, 1278–1288.
- Ritzi, R. W. (2000), Behavior of indicator variograms and transition probabilities in relation to the variance in lengths of hydrofacies, *Water Resour. Res.*, *36*(11), 3375–3381.
- Rojas, R., L. Feyen, and A. Dassargues (2008), Conceptual model uncertainty in groundwater modeling: Combining generalized likelihood uncertainty estimation and bayesian model averaging, *Water Resour. Res.*, *44*, W12418, doi:10.1029/2008WR006908.
- Sakaki, T., C. C. Fripiat, M. Komatsu, and T. H. Illangasekare (2009), On the value of lithofacies data for improving groundwater flow model accuracy in a three-dimensional laboratory-scale synthetic aquifer, *Water Resour. Res.*, *45*, W11404, doi:10.1029/2008WR007229.
- Schamper, C., E. Auken, and K. I. Sørensen (2014), Coil response inversion for very early time modeling of helicopter-borne time-domain em data and mapping of near-surface geological layers, *Geophys. Prospect.*, in press.
- Seifert, D., T. O. Sonnenborg, P. Scharling, and K. Hinsby (2008), Use of alternative conceptual models to assess the impact of a buried valley on groundwater vulnerability, *Hydrogeol. J.*, *16*(4), 659–674.
- Seifert, D., T. O. Sonnenborg, J. C. Refsgaard, A. L. Højberg, and L. Trolborg (2012), Assessment of hydrological model predictive ability given multiple conceptual geological models, *Water Resour. Res.*, *48*, W06503, doi:10.1029/2011WR011149.
- Selroos, J. O., D. D. Walker, A. Strom, B. Gylling, and S. Follin (2002), Comparison of alternative modelling approaches for groundwater flow in fractured rock, *J. Hydrol.*, *257*(1–4), 174–188.
- Sminchak, J. R., D. F. Dominic, and R. W. Ritzi (1996), Indicator geostatistical analysis of sand interconnections within a till, *Ground Water*, *34*(6), 1125–1131.
- Sophocleous, M. A., J. K. Koelliker, R. S. Govindaraju, T. Birdie, S. R. Ramireddygar, and S. P. Perkins (1999), Integrated numerical modeling for basin-wide water management: The case of the rattlesnake creek basin in south-central Kansas, *J. Hydrol.*, *214*(1–4), 179–196.
- Sørensen, K. I., and E. Auken (2004), SkyTEM—A new high-resolution helicopter transient electromagnetic system, *Explor. Geophys.*, *35*(3), 194–202.
- Strebelle, S. (2002), Conditional simulation of complex geological structures using multiple-point statistics, *Math. Geol.*, *34*(1), 1–21.
- Trolborg, L., J. C. Refsgaard, K. H. Jensen, and P. Engesgaard (2007), The importance of alternative conceptual models for simulation of concentrations in a multi-aquifer system, *Hydrogeol. J.*, *15*(5), 843–860.

- Trolborg, M., W. Nowak, N. Tuxen, P. L. Bjerg, R. Helmig, and P. J. Binning (2010), Uncertainty evaluation of mass discharge estimates from a contaminated site using a fully bayesian framework, *Water Resour. Res.*, *46*, W12552, doi:10.1029/2010WR009227.
- Viezzoli, A., E. Auken, and T. Munday (2009), Spatially constrained inversion for quasi 3D modelling of airborne electromagnetic data—An application for environmental assessment in the lower murray region of south Australia, *Explor. Geophys.*, *40*(2), 173–183.
- Viezzoli, A., F. Jørgensen, and C. Sørensen (2013), Flawed processing of airborne em data affecting hydrogeological interpretation, *Ground Water*, *51*(2), 191–202.
- Ward, S. H., and G. W. Hohmann (1988), *Electromagnetic Theory for Geophysical Applications*, SEG Publ., Littleton, Colo.
- Weissmann, G. S., and G. E. Fogg (1999), Multi-scale alluvial fan heterogeneity modeled with transition probability geostatistics in a sequence stratigraphic framework, *J. Hydrol.*, *226*(1-2), 48–65.
- Ye, M., and R. Khaleel (2008), A Markov Chain model for characterizing medium heterogeneity and sediment layering structure, *Water Resour. Res.*, *44*, W09427, doi:10.1029/2008WR006924.